

**THE INSTITUTE OF PAPER CHEMISTRY, APPLETON, WISCONSIN**

**IPC TECHNICAL PAPER SERIES  
NUMBER 283**

**THE INFLUENCE OF MOISTURE AND TEMPERATURE ON THE ULTRASONIC  
VISCOELASTIC PROPERTIES OF CELLULOSE**

**B. J. BERGER, C. C. HABEGER, AND B. M. PANKONIN**

**APRIL, 1988**

**The Influence of Moisture and Temperature on the Ultrasonic  
Viscoelastic Properties of Cellulose**

**B. J. Berger, C. C. Habeger, and B. M. Pankonin**

Portions of this work were used by BJB as partial fulfillment of the requirements for the Ph.D. degree at The Institute of Paper Chemistry. This paper has been submitted for consideration for publication in the Journal of Pulp and Paper Science

**Copyright, 1988, by The Institute of Paper Chemistry**

**For Members Only**

**NOTICE & DISCLAIMER**

The Institute of Paper Chemistry (IPC) has provided a high standard of professional service and has exerted its best efforts within the time and funds available for this project. The information and conclusions are advisory and are intended only for the internal use by any company who may receive this report. Each company must decide for itself the best approach to solving any problems it may have and how, or whether, this reported information should be considered in its approach.

IPC does not recommend particular products, procedures, materials, or services. These are included only in the interest of completeness within a laboratory context and budgetary constraint. Actual products, procedures, materials, and services used may differ and are peculiar to the operations of each company.

In no event shall IPC or its employees and agents have any obligation or liability for damages, including, but not limited to, consequential damages, arising out of or in connection with any company's use of, or inability to use, the reported information. IPC provides no warranty or guaranty of results.

# The Influence of Moisture and Temperature on the Ultrasonic Viscoelastic Properties of Cellulose

by B. J. Berger, C. C. Habeger, and B. M. Pankonin

## Abstract

Three ultrasonic techniques were used to measure mass specific elastic parameters for several papers and cellophanes as a function of temperature and moisture. The results of these measurements along with loss tangent values from one of the techniques are presented. Linear moisture-specific modulus and temperature-specific modulus relations were found for the temperature-moisture ranges likely to occur at the dry end of a paper machine. The resulting regression coefficients are given to assist those interested in environmental compensation of on-line ultrasonic modulus measurements. Significant deviations from linearity are reported over extended moisture and temperature ranges. These results are compared with lower frequency measurements and other ultrasonic data. The influences of moisture, temperature, and frequency on the viscoelastic parameters of cellulosic materials are discussed in some detail in terms of thermal relaxation processes.

## Introduction

The objective of this paper is to document the effects of environmental conditions on the loss tangent and the mass specific elastic moduli of cellulose measured at ultrasonic frequencies. The data are presented primarily as an aid for people engaged in nondestructive testing of paper with ultrasound. On-line ultrasonic testing can provide useful indicators of paper quality only if the measurements are adjusted for variations with moisture and temperature [1];

---

The Institute of Paper Chemistry, P.O. Box 1039, Appleton, WI, 54912.

therefore, it is important to establish a valid strategy for converting on-machine readings to the corresponding values at a standard condition. We argue in this paper that the correction algorithm can be simple, since the modulus depends linearly on temperature and moisture for the circumstances most commonly experienced on-machine. In addition to supplying practical experimental results, we use the established concept of thermally activated transitions to discuss the observed dependencies of the linear mechanical properties of cellulose on moisture, temperature, and frequency.

### **Background**

Since many people in the North American paper industry do not think of the linear physical properties of cellulose in terms of thermal relaxations, we take this opportunity to briefly review the thermal transition model of polymer compliance and its application to cellulose. To begin with, one should picture the molecules in the noncrystalline regions as having an equilibrium (or at least a quasi-equilibrium) distribution of conformations. A conformation is a collection of energy states that are separated from other conformations by energy barriers considerably greater than  $kT$  (Boltzman's constant times the absolute temperature). The equilibrium distribution can be altered by the application of external mechanical or electromagnetic stresses. The stresses shift the energies of the molecular states in such a way that the states in compliance with the stress decrease in energy relative to those states out of compliance. This creates a new Boltzman distribution of the molecular states, with a larger relative population in those states that comply with the stresses. When stresses are small, the energy shifts, the magnitude of the redistribution, and the resulting macroscopic compliance are proportional to the stresses.

After a polymer is stressed, the redistribution of states within each conformation occurs very rapidly, producing an immediate elastic response. However, the time required for molecular redistributions between conformations is significant. In order to effect a transfer between conformations, random thermal exchanges must proceed until energy, sufficient to surmount the potential barrier, is absorbed. For a step change in stress, switching between conformations proceeds exponentially with a time constant,  $\tau$ , called the relaxation time. Using Eyring's absolute rate theory, the relaxation time can be related to the absolute temperature,  $T$ , and the smaller of the two free energy differences,  $G$ , between the conformation states and the activated states at the top of the barrier as in Eqn. (1) [2].

$$1/\tau = (kT/h)e^{-G/kT} \quad (1)$$

If plausible assumptions concerning the activated and conformation states are made, the following order of magnitude approximation for  $\tau$  can be made [3].

$$1/\tau \approx 2\nu e^{-V/kT} \quad (2)$$

where  $V$  (the activation energy) is the height of the energy barrier and  $\nu$  is the frequency of the molecular vibration corresponding to the motion that leads to escape from the potential well. Therefore, a compliance resulting from motions between conformations requires a thermal relaxation time that depends exponentially on the temperature and the activation energy.

Any time-dependent stress can be expressed as a summation of sinusoidal components, and the complete linear response of a material is the linear superposition of the responses of the components. Thus, a description in terms of sinusoidal stresses of arbitrary frequency is sufficient to determine the

general linear behavior of a material. In the linear region, a sinusoidal stress produces a sinusoidal strain. However, when a single thermal transition is active, the magnitude and phase of the ratio between stress and strain change with frequency. At frequencies much greater than  $1/\tau$ , the thermal transition does not participate in the compliance. At frequencies far below  $1/\tau$ , the thermal transition keeps up with the stress and contributes fully to the compliance. In both cases, stress and strain are in phase, and the material is elastic. At frequencies of the order of  $1/\tau$ , the phase angle of the strain lags the phase of the stress; the compliance is intermediate; energy is dissipated in each cycle; and the material is viscoelastic. The transition frequency ( $f_0$ ), which can be defined as the frequency of the loss tangent maximum, is a function of temperature and is approximately equal to  $1/\tau$ . If  $f_0$  is proportional to  $1/\tau$  and Eqn. (2) is accurate, an Arrhenius plot of  $\ln(f_0)$  vs.  $1/T$  is linear with a slope of  $-V/k$ . Since  $f_0$  is temperature dependent, transitions can also be observed at constant frequency by varying temperature. At low temperatures the relaxation does not contribute to compliance; at a higher temperatures it does; and a frequency-dependent relaxation temperature can be defined in the transition region. Notice that the change in  $f_0$  with temperature increases with activation energy. In other words, the temperature of a thermal transition is less frequency dependent when activation energy is large.

Of course, in real polymers there can be more than one thermal transition, and each transition can have a distribution of activation energies. Therefore, a graph of loss tangent vs. frequency would exhibit a number of broad (possibly overlapping) peaks. Consider a hypothetical polymer with two transitions, each governed by Eqn. (2). The graph of  $\ln(f_0)$  vs.  $1/T$  would have a straight line for each relaxation and would resemble Figure 1. Experiments

conducted at frequencies and temperatures, represented by points in Figure 1 that are well to the right of a transition line, do not participate in that relaxation; those well to the left do participate; and those near a transition line partially participate. As  $1/T$  approaches zero, the  $f_0$ 's extrapolate to roughly the frequency of their corresponding vibrations. These vibrations occur at infrared frequencies (around  $10^{13}$  to  $10^{14}$  Hz), and from the much lower frequencies where normal mechanical measurements are made, the two lines in Figure 1 appear to intercept the  $\ln(f_0)$  axis at about the same point. The line representing the transition with the larger activation energy has the slope of largest magnitude. Therefore, if temperature is scanned at constant frequency, the transition at the higher temperature will have the larger activation energy. Also, the transitions will be closer together in inverse temperature at higher frequency scans, making the individual loss tangent peaks more distinct at lower frequencies.

Figure 1 here

Moisture generally "plasticizes" thermal transitions. The addition of water, or any other low molecular weight substance, to the noncrystalline region increases the free volume in the polymeric structure. This usually reduces the activation energy of the transitions, increases the intensity of their relaxation, and moves the transitions to lower temperatures. However, moisture can "antiplasticize" [4] secondary transitions in hydrophilic polymers such as nylon [5] and cellulose [6]. In these cases, water hinders the motion of the polymer segment involved in the transition. Thus, the transition is transformed into a higher temperature, higher activation energy relaxation, which could require motion of a segment-water complex. Therefore, the addition of moisture diminishes the magnitude of a low temperature relaxation, as it augments that of

a higher temperature relaxation. At temperature-frequency combinations between the original transition and the moisture induced transition, the addition of moisture can actually increase stiffness and tensile strength [5,6]. The moisture induced transition is effectively plasticized by water, in that its transition temperature decreases and the magnitude of its relaxation increases as moisture is added.

Thermal relaxations in cellulose and in cellulose-water systems have been studied extensively. A broad, low-temperature relaxation in dry cellulose (named the  $\gamma$  transition) has been measured with mechanical [6,7,8,9], dielectric [7,10,11,12,13,14], NMR [10], and piezoelectric [14] techniques. It occurs at about  $-95^{\circ}\text{C}$  for experiments conducted at 1 Hz and has a molar activation energy of about 12 kcal/mole. This extrapolates to a transition temperature of about  $-10^{\circ}\text{C}$  at an ultrasonic frequency of 60 kHz. Many investigators (Bradley and Carr [6] and Nishinari and Fukada [14] in particular) argue that the  $\gamma$  relaxation is produced by rotations of the methylol side-groups of the glucose chains in the noncrystalline regions. The  $\gamma$  relaxation is a secondary transition. This means that its motion is localized to small segments of the polymer chain, it has a relatively low activation energy, it is observed at low temperature, and it is comparatively weak. In addition to the  $\gamma$  relaxation, the onset of an  $\alpha$  transition in dry cellulose is well documented [6,7]. This is a strong, high-temperature relaxation which has loosely been described as a glass transition in the noncrystalline region. Its activation energy is more than 100 kcal/mole, and it requires the motion of larger segments of the cellulose backbone. The  $\alpha$  transition temperature is above  $200^{\circ}\text{C}$ ; therefore, cellulose degrades thermally before the peak in the loss tangent vs. temperature plot is fully developed. The inception temperature of the flank of the  $\alpha$  transition, which is around room

temperature, is not very sensitive to frequency because of the large activation energy.

Moisture has profound influences on the thermal transitions of cellulose. The low temperature behavior is a classic example of antiplasticization by water. Small amounts of water decrease the intensity of the  $\gamma$  peak [6,8,11,14] and generate a new peak [6,8,9,11,14], called the  $\beta$  relaxation. Continued water sorption intensifies the  $\beta$  peak and attenuates the  $\gamma$  peak. Moisture addition reduces the transition temperature of the  $\beta$  relaxation more effectively than that of the  $\gamma$  relaxation. The  $\beta$  relaxation is at a higher temperature (around  $-70^{\circ}\text{C}$  at 1 Hz and 7.3% moisture in cellophane [6]) and has a higher activation energy (about 16.5 kcal/mole [6] in cellophane with 7.3% moisture) than the  $\gamma$  relaxation. Stiffness measurements, made at a temperature combination between the  $\gamma$  and  $\beta$  relaxations, demonstrate that water can increase the stiffness of cellulose [6,15]. At a moisture content corresponding to approximately one water molecule per methylol group in the noncrystalline region, the  $\gamma$  relaxation disappears, and the  $\beta$  relaxation remains as the only secondary transition [6]. This, of course, is all taken as evidence that the  $\beta$  relaxation is due to the rotation of a methylol-water complex [6,8].

The  $\alpha$  relaxation is effectively plasticized by water. The increase in free volume, afforded by moisture sorption, lowers the activation energy (and thereby the transition temperature) of the  $\alpha$  relaxation and increases its intensity. At moderate moisture contents, the low-temperature flank of  $\alpha$  relaxation begins to have significant influence on room-temperature experiments. In fact, the well known sensitivity of the room-temperature physical properties of cellulose to moisture (above about 5% moisture content) is believed to be a result of the plasticization of the  $\alpha$  relaxation by water.

## Experimental Procedures

Resonance and time-of-flight techniques were used to measure viscoelastic parameters of cellulosic materials at ultrasonic frequencies. Several commercial samples were tested including two different cellophanes, typing paper, blotter paper, an alkaline made bond paper, and two different basis weight linerboards. Although samples were chosen somewhat arbitrarily, an effort was made to include a wide variety of materials.

The operation of the resonance apparatus is described in detail in another publication [15] and briefly outlined below. The basic approach, which is diagrammed as a part of Figure 2, is to determine the mass specific elastic modulus ( $E/\rho$ ) and the loss tangent ( $\tan\delta$ ) from the frequency dependence of the standing wave vibrations in a narrow strip. The strip is coupled between a pair of ceramic piezoelectric transducers; one transducer is excited with a sinusoidal voltage; and the resulting signal at the other transducer is measured as a function of frequency. The transducers are 5 x 5 mm squares of a 2 mm thick sheet of a lead zirconate titanate ceramic (Edo Western EC-65 PZT). The piezoelectric is polarized in the thickness direction with the top and bottom surfaces acting as electrodes. The shield and active leads of a miniature coaxial cable are soldered to opposite electrodes of the transducers to provide electrical contact and physical support. Each cable is threaded through an oversized hole in an aluminum block. The cable is held in the block and acoustically isolated from the block with a silicone potting compound. The aluminum blocks are mounted on a track which allows the transducer separation to be adjusted. The test samples are cut with a razor blade to lengths of 4-7 cm and widths of approximately 0.2 cm and are glued between the transducers using a thin layer of a cyanoacrylate adhesive.

Figure 2 here

The transmitter excitation signal is generated by a Hewlett Packard 3325A Frequency Synthesizer. The frequency and amplitude of the synthesizer output are controlled by a Texas Instruments 9900 Microcomputer over an I.E.E.E. bus. The sinusoidal voltage across the transmitter causes it to expand in the transverse direction exciting longitudinal vibrations in the sample. These vibrations are converted to an electrical signal by the transducer at the other end of the sample. The signal then goes to an Ithaco 393 Lock-In Amplifier which functions as a narrow band-pass filter and amplifier at the frequency generated by the synthesizer. The analog output from the lock-in is routed to an analog to digital converter in the microcomputer and to the Y-axis of an X-Y plotter. The X-axis of the plotter is connected to an output from the synthesizer that is proportional to the frequency.

When the frequency of the synthesizer is swept, the X-Y plotter generates a graph of the lock-in amplitude vs. frequency. If the sample is properly attached to the transducers, the graph contains sharp, regularly-spaced resonance peaks. A typical spectrum from a well-bonded sample is presented in Figure 3. The shapes of these peaks and their locations are used to calculate the sample loss tangent and mass specific Young's modulus. Mass specific Young's modulus is equal to  $2l_s f_{\max}/(m+1)$ , where  $m$  is the order of the harmonic,  $l_s$  is the sample length, and  $f_{\max}$  is the frequency of the resonance peak. The loss tangent equals  $\Delta f/f_{\max}$  where  $\Delta f$  is the frequency width of the peak at  $1/\sqrt{2}$  of the maximum amplitude. By adjusting the sample length and concentrating on different harmonics, the frequency range of the experiment can be extended from 10 to 100 kHz. Once proper sample coupling is demonstrated by a well-formed spectrum, operation of the synthesizer is controlled by the microcomputer.

An optimization program supervises a sequence of synthesizer frequencies and lock-in output readings which allows the calculation of  $E/\rho$  and  $\tan\delta$ . These quantities are printed out and sent periodically to the mainframe computer.

Figure 3 here

Since the value of the sample length is used to calculate the strip modulus, length variance with moisture and temperature must be considered. Dimensional changes of cellulose with temperature are small [16] and are ignored. However, there is a significant linear [17] dependence of length on moisture, and an appropriate correction must be made. This was done by subjecting the samples to 18% R.H. and 92% R.H. at room-temperature in a separate humidity chamber that permitted the lengths to be measured accurately under small loads. The two corresponding moisture contents were calculated and a linear relation between length and moisture was determined. The necessary adjustments to  $E/\rho$  were performed at the completion of the runs.

The time-of-flight technique is a modification of a two-transducer method described elsewhere [18]. That apparatus translated one transducer in order to achieve time-of-flight measurements at two different separations. Because of the difficulties in manipulating transducers in an environmental chamber, an apparatus with three stationary transducers was used for this temperature-moisture dependence study. The three-transducer method is also diagrammed in Figure 2 and briefly discussed below, with emphasis on the special considerations encountered with fixed transducers.

As with the two-transducer time-of-flight method, piezoelectric bender transducers are used. They are mounted in-line to a rigid frame. The frame is of open construction so that air can circulate freely around the sample. The middle transducer is 30 cm from one end transducer and 60 cm from the other.

The mounting frame is part of a larger assembly designed to clamp the sample vertically between the transducers and neoprene backings. The clamping pressure can be adjusted by changing the length of a spring which holds the transducers to the backings.

During operation, the outer two transducers act as transmitters and the inner one as a receiver. The measurement starts with a pulse from an Apple II Plus Computer. This triggers a signal generator to send a one-cycle, 80 kHz electrical pulse to the near transmitter. The transmitter oscillates in the plane of the paper. If the transducers are aligned so that this oscillation is parallel to their separation, a longitudinal plate wave is generated in the sheet and detected by the receiver. If oscillation is perpendicular to transducer separation, a shear wave results. In either case, the received signal is amplified by a Panametrics 505AE Preamplifier, sent to a Biomation 805 Transient Recorder for analog-to-digital conversion, and transferred to the Apple for data analysis. Next, the far transmitter is excited and the data gathering process is repeated. Signal-to-noise ratio is improved by taking multiple near and far signals and programming the computer to perform digital signal averaging.

The resulting signals are roughly sinusoidal waves with initial dead times. The Apple determines a time-of-flight difference for the two spacings by finding the maximum in the cross-correlation function of the first half-cycles of the two signals. The difference in the distances between the transducer spacings is then divided by this time in order to determine a time-of-flight velocity. If thin strips are tested with the bender transducers aligned for longitudinal wave generation, the velocity squared is equal to the mass specific Young's modulus,  $E/\rho$ . However, if sheets whose width is large compared to the wavelength of sound are tested, the velocity squared is a mass specific planar stiffness,  $C/\rho$ .

The planar stiffness,  $C$ , is equal to  $E/(1-\nu_{12}\nu_{21})$ , where the  $\nu_{ij}$ 's are the in-plane Poisson ratios. If the transducers are oriented for shear waves, the velocity squared in the extended sheet is  $G/\rho$ , where  $G$  is the in-plane shear modulus. In comparison with the two-transducer approach, this technique is handicapped in that measurement of an accurate velocity depends on matching the transmitter transducers and their coupling to the sample. Therefore, absolute values are somewhat in question, but relative variations generated by moisture and temperature changes are valid.

In an earlier publication [15], we described an environmental chamber suitable for making below room temperature measurements with the resonant apparatus. It was also capable of performing higher temperature measurements on dry samples, but was inappropriate for high temperature work on moist samples. In addition, it was too small to contain a time-of-flight instrument which could give transverse as well as longitudinal velocities. Therefore, in order to study the effects of temperature and moisture on the ultrasonic moduli at conditions relevant to on-line testing, we prepared a second environmental chamber. This is a modification of a Blue M Model CF Temperature/Humidity Chamber. The air temperature in this oven can be controlled at any value between ambient and 105°C. Relative humidity depends on the temperature in a cooling bath at the bottom of the chamber. This is determined by the temperature and flow rate of water into the bath, the level of the bath, and the heat supplied by a heating element submerged in the bath. The bath level is fixed by adjusting the height of an overflow pipe, and a valve controls the flow rate into the oven. Cooling water is supplied by a 70 gallon insulated tank of ice-water. The water flows by gravity from the tank into the oven bath where it is heated. It eventually flows out the overflow pipe and into a 2 gallon

holding tank. A recirculating pump periodically returns this water to the ice tank. After modifying the oven, a special fan, which could be switched rapidly on and off by the Apple, was installed at the top of the chamber. The fan forces air past the bath and insures that humidity and temperature are uniform throughout the chamber.

Moisture content is determined by weighing a sample, similar to the one being tested, with a Metler PE 360 Balance which is capable of weighing hanging objects. The balance is isolated from oven vibrations by placing it on a platform which is cantilevered above the oven. A thin wire sample holder attaches to the bottom of the balance and extends, through a small hole, into the oven. A heating lamp is aimed at the hole to insure that there is no condensation on the sample holder. There is a digital interface between the balance and the Apple, and the computer can obtain sample weight at any time by stopping the fan and reading the balance. Moisture content, which we define as water weight divided by total weight, can later be calculated from the oven-dry weight of the weighing sample.

Temperature is measured using a Fluke 2170A Digital Thermometer and 75  $\mu$ m diameter copper-constantan thermocouples. There is a digital interface between the thermometer and the Apple. As was the case for moisture measurements, temperature of a sample similar to the one being tested is measured. This is accomplished by imbedding the thermocouple in a thick sample or by sandwiching the thermocouple between two layers of a thin sample.

A typical run, in which temperature is constant and moisture changes slowly, proceeds as follows. The dry bulb heating element is adjusted to obtain the desired air temperature. When the oven reaches this temperature, the valve controlling the flow of the cooling water is fully opened. This produces a

minimum possible relative humidity in the oven at the given air temperature and bath depth. After stabilizing the oven for an hour, the flow control valve is closed. This causes the water in the cooling bath to slowly heat up and the relative humidity in the oven to increase. Depending upon the air temperature in the oven and the depth of the bath, this heating period can take from several hours to a day. Eventually the bath temperature reaches a maximum and the sample moisture content attains its maximum value. Due to a slow loss of moisture from the system, water in the bath continues to evaporate, and relative humidity begins to fall. As the bath dries up completely, a moisture content that is close to the one obtained originally at maximum flow rate of cooling water, is approached. In this manner, the test samples are slowly cycled from dry to wet to dry. In order to stabilize the sample by relieving dried-in stresses, the oven is cycled two times before testing. During a test cycle, sample temperature and mass, the frequency of the strip resonance, the peak width of the resonance, and the time-of-flight velocity are all regularly measured. These measurements are used to calculate the equilibrium moisture dependence of the sample modulus and loss tangent during sorption and desorption. After a cycle is complete, additional cycles at the same temperature can be performed, or the temperature can be altered and different modulus vs. moisture plots generated.

## Results

The Blue M oven was used to make specific elastic modulus measurements with all three techniques on cellophane and a variety of papers in a temperature and moisture regime representative of conditions at the dry end of a paper machine. Strip resonance results for a 38  $\mu$ m thick unplasticized cellophane film, made by BCL cellophane, and designated as 550 P00, are presented in Figure 4. Notice

that in this range the moisture dependence of the specific modulus is nearly linear. Also, temperature changes are equivalent to uniform horizontal shifts in the modulus plots, and the magnitude of the shift is proportional to the temperature difference. This permits the construction of the master curve presented in Figure 5 for the cellophane at 55°C. If care is taken not to exceed the range of the experiments, specific moduli plots at other temperatures can be generated by shifting the master curve -0.088% moisture for every degree centigrade above 55°C.

Figures 4 and 5 here

As described in the experimental procedures section, oven modulus data were obtained through slow sorption and desorption. However, no significant moisture-modulus hysteresis was observed. The correspondence of sorption and desorption moduli, shown in Figure 4, is representative of results from the other samples. The lack of a moisture-modulus hysteresis was also reported from load-elongation experiments by Higgins [19] and Salmen and Back [20]. The present study extends their observation to higher frequency experiments. Also, since our tests are nondestructive and a single sample is used over the entire range, scatter due to sample variability is precluded, and the conclusion is made with more confidence. The lack of a moisture-modulus hysteresis is interesting in that a hysteresis is observed in the dielectric measurements of Dusoiu [21]. In his microwave permittivity study, a moisture-dielectric constant hysteresis loop was found indicating that water is on average bonded differently in sorption and desorption at the same moisture content. The absence of a moisture-modulus hysteresis probably arises from the lesser importance of the mobility of the water molecules in mechanical compliance.

The linear dependence of specific modulus on temperature and moisture, which was just described for the cellophane, was observed for the other samples tested in this regime. The results are presented in Table 1 in terms of regression coefficients for the least squares fit to linear relations of the form,  $V^2 = \beta_M(M-M_0) + \beta_T(T-T_0) + V_0^2$ . The symbol M represents the percent moisture content;  $M_0$  is the percent moisture content at 50% R.H. arrived at through sorption; T is the absolute temperature; and  $T_0$  is 25°C. The least squares regression coefficients are represented by  $\beta_M$ ,  $\beta_T$ , and  $V_0^2$ . Notice that multiple MD longitudinal runs are presented for the blotter paper and the linerboard. Different samples were tested each time, some with the time-of-flight and some with the resonance technique. Comparing coefficients for these runs gives the reader a feeling for the sample variability, the repeatability of the techniques, and the consistency of results between techniques.

Table 1 here

In addition to the consistently large values for the squared correlation coefficients ( $r^2$ ), there are other interesting observations to be made in Table 1. Notice that the longitudinal specific modulus of linerboard in the MD is significantly less affected by temperature and moisture than the shear and CD specific longitudinal moduli in linerboard. Also, for cellophane and typing paper the shear mode is more environmentally sensitive than the longitudinal mode. The greater stability in MD longitudinal modulus is presumably a result of the greater concentration of stresses in crystalline regions during propagation of this mode. Another observation is that the values of  $\beta_M$  and  $\beta_T$  are positively correlated in such a way that  $\beta_M/\beta_T$  (the temperature rise in degrees centigrade that causes a specific modulus change equal to that produced by a one percent moisture increase) is remarkably independent of the sample tested and

the mode propagated. The average value of  $\beta_M/\beta_T$  is  $12.3^\circ\text{C}/\%$ , with a standard deviation of  $1.2^\circ\text{C}/\%$ .

The range of sample moisture contents that can be realized in the oven depends on temperature. The maximum and minimum moisture contents measured at each temperature are listed in Table 2 for each sample. The temperatures and moistures at the reel of a paper machine, where on-line ultrasonic measurements are made, usually fall within the extremes listed in Table 2. The existence of the linear moisture-modulus and temperature-modulus relationships, cited in Table 1, is therefore fortuitous, since by measuring sample specific modulus, temperature, and moisture on-machine and applying linear correction factors, the specific modulus at a standard environmental condition can be calculated.

Table 2 here

It must be emphasized that even though ultrasonic specific moduli vary linearly with moisture and temperature over the range available in our oven, linear variance of modulus with environment is not a universal property of cellulosic materials. At the oven conditions, moisture and temperature primarily alter the mechanical compliance of cellulose through their influence on the low temperature flank of a single transition (the  $\alpha$  relaxation). Over the limited range experienced in the oven, this happens to lead to a linear behavior. At lower temperatures, complex interactions between environmental conditions and secondary transitions result in large deviations from linearity. Figure 6 is an illustration of the more general behavior of cellulose. Here, data obtained from the Du Pont PUD0-134 cellophane taken with the resonant strip technique in the low-temperature environmental chamber [15] are extended by resonant strip measurements made in the oven. The oven data are represented by lines calculated from the Table 1 regression coefficients at the five moisture contents

encountered in the low-temperature chamber. Notice particularly, the intersections of the specific modulus vs. temperature curves in Figure 6. This is a manifestation of the antiplasticizing effect of water on the secondary relaxations in cellulose. At temperatures below the  $\beta$  relaxation, repression of  $\gamma$  relaxation by water leads to an increase in specific modulus. At higher temperatures, the  $\beta$  relaxation and the onset of the  $\alpha$  relaxation are encountered, and moisture has the more common consequence of decreasing the modulus.

Figure 6 here

Additional insight into moisture-temperature-modulus relationships can be obtained by studying the loss tangent vs. inverse temperature curves in Figure 7. As was Figure 6, this is a composite of data taken in the low-temperature chamber and in the oven. In order to get the oven loss tangents to coincide with the low-temperature data, the loss tangents measured in the oven were uniformly decreased by 0.008. This resulted in similar values at the two moisture-temperature conditions common to both studies ( $378^\circ\text{K} - 0\%$  moisture,  $298^\circ\text{K} - 7.9\%$  moisture). We speculate that artificially high oven loss tangents result from transducer-sample coupling degradation occurring when the humidity of the oven is cycled in an attempt to stabilize the sample, as described earlier. Increases in loss tangents determinations are routinely observed when samples are moisture cycled. Since the low-temperature chamber was not cycled after sample bonding, we assume that it yields the more reliable absolute values of loss tangent. Notice the  $\tan \delta$  curve in Figure 7 for the dry cellophane. Here, the  $\gamma$  relaxation produces a distinct peak at about  $-10^\circ\text{C}$ . Addition of the first moisture increments decreases the intensity of this peak and shifts it to a higher temperature. Further moisture additions increase the peak height and move it to lower temperatures. This is understood in terms of the antiplasticization of

the  $\gamma$  relaxation by water. The water first converts the  $\gamma$  transition to a higher temperature  $\beta$  transition and then effectively plasticizes the  $\beta$  transition. Separate maxima are not observed for these relaxations, since their overlap is too great at ultrasonic frequencies. The dry loss tangent data in Figure 7 also contain evidence for the  $\alpha$  relaxation. This is seen as an upturn in the loss tangent curve just above room temperature. The onset of this transition is steadily enhanced by moisture addition.

Figure 7 here

### Discussion

Since ultrasonic modulus measurements are conducted at higher frequencies than the standard mechanical tests, they experience the secondary transitions at higher temperatures and find them more closely spaced in temperature. This is demonstrated by comparing Figure 7 with the loss tangent data for a 25  $\mu\text{m}$  thick unplasticized cellophane at 11 Hz published by Bradley and Carr [6]. Their cellophane, PUDO-193, was also obtained from Du Pont and differs from the Figure 7 sample in thickness. Their Figure 1 is reproduced by permission from the publisher as our Figure 8. In the Bradley and Carr plot at 2.8% moisture, separate peaks are generated by the  $\beta$  and  $\gamma$  transitions. At 4.1 and 7.3% moistures the  $\gamma$  transition is eclipsed by the  $\beta$  transition, while at 0.34% moisture the  $\gamma$  transition dominates and the  $\beta$  is barely discernible. Since the  $\beta$  relaxation has a higher activation energy than the  $\gamma$  relaxation, only one peak is observed for ultrasonic loss tangent data at intermediate moistures. At these frequencies, the  $\beta$  and  $\gamma$  relaxations are too close in temperature to be displayed as distinct peaks. Since the  $\alpha$  relaxation has by far the largest activation energy, the onset temperature of the  $\alpha$  peak is not very sensitive to frequency. In summary, ultrasonic and low frequency modulus measurements differ

because at higher frequency viscoelastic relaxations are more closely spaced and occur at higher temperature. This leads to a higher ultrasonic modulus at the same temperature, as there is less time available for viscoelastic relaxations.

Figure 8 here

Dry loss tangent data from Figures 7 and 8 can be used to determine an activation energy for the  $\gamma$  transition. The peak is seen to shift from  $-80^{\circ}\text{C}$  to  $-10^{\circ}\text{C}$  when going from 11 Hz to 60 kHz. This results in a calculated activation energy of around 12 kcal/mol. A rough estimate of the activation energy for the  $\alpha$  transition can also be obtained from dry data (assuming temperature shifts of troughs are similar to those of peaks). At ultrasonic frequencies the onset of the  $\alpha$  transition occurs at around  $90^{\circ}\text{C}$ . The corresponding onset for the Bradley and Carr data is around  $70^{\circ}\text{C}$  resulting in a calculated activation energy of slightly over 100 kcal/mol.

A time-temperature superposition argument can be used to rationalize the differences in modulus values obtained using ultrasonic and lower frequency techniques. The specific modulus of dry cellophane measured ultrasonically at room temperature ( $295^{\circ}\text{K}$ ) is approximately  $13.5 \times 10^{10} \text{ cm}^2/\text{sec}^2$ . Assuming a density of 1.45 g/cc for cellophane, this value is approximately  $10 \times 10^{10} \text{ cm}^2/\text{sec}^2$  for Bradley and Carr [6]. When compared at an equivalent temperature, results are much closer. If an activation energy of 12 kcal/mole for the  $\gamma$  relaxation is used, ultrasonic data at room temperature are equivalent to 11 Hz data at  $210^{\circ}\text{K}$ . At this temperature, the Bradley and Carr specific modulus is approximately  $13.8 \times 10^{10} \text{ cm}^2/\text{sec}^2$ .

In addition to the present study, other reports of the effects of moisture on the room temperature ultrasonic modulus of paper are available. These

results, along with some published low frequency moisture-moduli data, are summarized in Table 3. For the sake of comparison, literature data with moistures above 20% were not used. We also attempted to express all results in terms of the parameters described for Table 1. This lead to some difficulties, however. To start with, there was no straightforward way of determining the appropriate  $r^2$  values for some of the studies. This is because raw data were not available, and  $r^2$  had to be estimated by pulling representative points from published curves. These correlation coefficients, which are placed in parentheses, have limited statistical significance, but do give an indication of the linearity of data. Also,  $M_0$ , the moisture content at 50% R.H., was not always presented, and some  $M_0$  numbers were estimated from known values of similar papers. Finally, since density was not always reported, modulus rather than specific modulus was listed for the low frequency work and a different moisture sensitivity parameter,  $\beta_{M1}$  was calculated. However, as density is not overly sensitive to moisture at contents less than 20%,  $\beta_M/V_0^2$ , is approximately equal to  $\beta_{M1}/E_0^2$  and meaningful comparisons of the relative moisture dependence of modulus and specific modulus at different frequencies can be made. To illustrate this, the ultrasonic data from sample XII is presented in both forms. Notice that the relative sensitivities of specific modulus and modulus to moisture, -0.043/% and -0.045/%, are nearly equal. Sample XII is also the only sample for which modulus is listed in both frequency regimes. The approximately 25% decrease, observed in shifting frequency from ultrasonic to load-elongation measurements, is typical of cellulosic materials.

Table 3 here

From the high  $r^2$  values in Table 3, it appears that linear relationships are appropriate characterizations of high and low frequency room temperature moisture-modulus measurements. However, results, extending to higher moisture

levels, conform better to an exponential dependence of modulus to moisture at both low [22] and high [23,24] frequencies. In addition, a decrease in the moisture sensitivity of room temperature modulus below about 5% moisture has been reported at low [9,19,20], and high [8] frequencies. Even though one study [25] failed to document this modulus plateau at low moisture, considerations of the behavior of secondary relaxations in cellulose lead us to believe it is a real phenomenon. At low frequency the  $\gamma$  and  $\beta$  relaxation are complete at room temperature. Therefore, the conversion of the  $\gamma$  relaxation to the  $\beta$  relaxation by initial moisture addition has little effect on low frequency measurements. As moisture content is increased further, however, the onset of the  $\alpha$  transition protrudes into the low frequency, room temperature domain. This results in an increase in loss tangent and a greater sensitivity of modulus to moisture. Our ultrasonic measurements also reveal a deviation from linearity at room temperature and low moisture content (see Figure 6), but the action is more complex at high frequency. Here the  $\beta$  and  $\gamma$  transitions are not complete at room temperature, and initial moisture increments can have an antiplasticizing effect. This, along with the movement of the onset of the  $\alpha$  transition to a somewhat higher temperature, augments the difference between low and moderate moisture behavior at high frequency. This phenomenon did not cause deviations from linearity in our oven measurements, since the dry data were all taken above room temperature where  $\beta$  was nearly complete and  $\alpha$  was active.

An examination of moisture sensitivity parameters from Table 3 brings out some interesting points. First of all, with one exception, the normalized values of  $\beta_M$  (or  $\beta_{M1}$ ) in each regime are remarkably consistent. Like measurements are of roughly the same value, and the CD longitudinal and shear slopes are lower than the MD longitudinal values from the same sample. The one exception

to the consistency of results, sample XIV, is reported to have such a low slope that its validity is called into question. Notice also that the relative moisture sensitivity is significantly lower at ultrasonic frequencies. However, if  $\beta_{M1}$  is converted to  $\beta_M$  by a density multiplication, and if sensitivity is compared on an absolute basis, results are similar. For example, the  $\beta_M$  value for sample XII data is  $0.30 \text{ km}^2/\text{sec}^2/\%$  when measured at low frequencies and  $0.28 \text{ km}^2/\text{sec}^2/\%$  at ultrasonic frequencies.

The results in Table 3 can be interpreted in terms of the thermal relaxation model. At room temperature, the  $\alpha$  transition plays a dominant role in the environmental sensitivity of the physical properties of cellulose. In Figure 9, the  $\alpha$  transition is idealized as a standard linear solid. Notice that this produces a large linear regime in the plot of log frequency vs. modulus. The established principle of time-temperature superposition in polymeric materials [31] demonstrates that the changes produced by a shift in inverse temperature are often equivalent to a proportional change in the logarithm of the frequency. If we assume that the  $\alpha$  transition obeys an Arrhenius relationship and that moisture has a linear effect on the activation energy, then a moisture-log frequency equivalence also results. Although the above analysis relies on some admittedly tenuous assumptions, it does rationalize many of the observed results. At low test frequencies, initial moisture addition would be roughly equivalent to moving along the modulus, E, curve from a to b (see Figure 9) resulting in only minimal modulus changes. This would explain the reported low moisture sensitivity of modulus at low moistures. The more complex room temperature, moisture-ultrasonic modulus response seen at low moistures is due to the closer spacing of transitions at these frequencies. Therefore, unlike the low frequency case where other transitions are complete and the path from a to b is affected only by the  $\alpha$  transition response, the ultrasonic modulus is also

affected by the completion of the  $\beta$  and  $\gamma$  transitions. With continued moisture addition, a regime is encountered in which moisture and modulus are related nearly linearly (b to c). This helps explain the equivalence of low and high frequency  $\beta_{M1}$  and  $\beta_M$  values in Table 3. Ultrasonic data in this table would just be obtained higher along the line (closer to b) than low frequency data resulting in higher  $V_o^2$  (and  $E_o^2$ ) values. At even higher moisture addition levels, the relaxation nears completion and modulus begins to decrease at a decreasing rate (c to d), explaining the logarithmic modulus-moisture response reported at high moistures.

Figure 9 here

#### ACKNOWLEDGMENTS

Portions of this work were used by BJB as partial fulfillment of the requirements for the Ph.D. degree at The Institute of Paper Chemistry.

#### REFERENCES

1. HABEGER, C. C. and BAUM, G. A. Tappi, 69 (6): 106-111 (1986).
2. WARD, I. M. Mechanical Properties of Solid Polymers, (chapt. 7), Wiley-Interscience, New York (1970).
3. HILL, T. L. Introduction to Statistical Thermodynamics, (chapt. 11), Addison-Wesley, Reading, Mass. (1960).
4. JACKSON, W. J. and CALDWELL, J. R. Advan. Chem. Ser., 48: 185 (1965), J. Appl. Poly. Sci., 11: 211-244 (1967).
5. KOLARIK, J. and JANACEK, J. J. Polym. Sci., 16: 441-449 (1967).
6. BRADLEY, S. A. and CARR, S. H. J. Polym. Sci., Polym. Phys. Ed., 14: 111-124 (1976).
7. KLASON, C. and KUBAT, J. Svensk Papperstidning, 79 (15): 494-500 (1976).
8. KIMURA, M. and NAKANO, J. J. Polym. Sci. Polym. Lett. Ed., 14: 741-745 (1976).
9. STRATTON, R. A. J. Polym. Sci., Polym. Chem. Ed., 11: 535-544 (1973).
10. MIKHAILOV, G. P., ARTYUKOV, A. I., and SHEVELEV, V. A. Vysokomol. Soed., A11: 553 (1969).
11. SEIDMAN, R. and MASON, S. G. Can. J. Chem., 32: 744-762 (1954).
12. ABDEL MOTELEB, M. M., NAOUN, M. M., SHINOUDA, H. G., and RIZK, H. A. J. Polym. Sci., Polym. Chem. Ed., 20: 765-774 (1982).
13. NORIMOTO, M. and YAMADA, T. Wood Res., 52: 31-43 (1971).

14. NISHINARI, K. and FUKADA, F. J. Polym. Sci., Polym. Phys. Ed., 18: 1609-1619 (1980).
15. PANKONIN, B. M. and HABEGER, C. C. J. Poly. Sci., Polym. Phys. Ed., 26: 339-352 (1988).
16. KUBAT, J., MARTIN-LOF, S., and SOREMARK, C. Svensk Papperstidning, 72 (23): 763-767 (1969).
17. BYRD, V. L. Tappi, 55 (2): 247-252 (1972).
18. VAN ZUMMEREN, M. L., YOUNG, D. J., HABEGER, C. C., BAUM, G. A., and TRELEVEN, R. A. Ultrasonics, 25: 288-294 (1987).
19. HIGGINS, H. Appita, 12 (1): 1-17 (1958).
20. SALMEN, N. L. and BACK, E. L. Tappi, 63 (6): 117-120 (1980).
21. DUSOIU, N. C. R. Acad. Sci., B280 (24): 777-779 (1975).
22. HTUN, M., DE RUVO, A., and FELLERS, C. J. Appl. Poly. Sci., 30: 1597-1604 (1985).
23. CAULFIELD, D. and WEATHERWAX, F. Trans. Fibre-Water Interactions In Paper-Making, Oxford, 2: 741-758 (1977).
24. BYL, C. C. Master's Thesis, The Institute of Paper Chemistry, 1983.
25. RIEMEN, W. and KURATH, S. Tappi, 47 (10): 629-633 (1964).
26. BENSON, R. E. Tappi, 54 (5): 699-703 (1971).
27. BREZINSKI, J. P. Ph.D. Thesis, The Institute of Paper Chemistry, 1955.
28. AUSTIN, J. N. Master's Thesis, The Institute of Paper Chemistry, 1978.
29. CRAVER, J. and TAYLOR, D. Tappi, 48 (3): 142-147 (1965).
30. BAUM, G., BRENNAN, D., and HABEGER, C. Tappi, 64 (8): 97-101 (1981).
31. FERRY, J. D. Viscoelastic Properties of Solid Polymers, (Chapt. 11), John Wiley and Sons, New York (1980).

### Figure Captions

- Fig. 1. A hypothetical Arrhenius plot for a viscoelastic material with two thermal relaxations.
- Fig. 2. A schematic of the resonant and time-of-flight experiments enclosed in the variable humidity oven.
- Fig. 3. A typical trace from the X-Y plotter of the lock in amplifier response as a function of frequency. (The methods used for the modulus and loss tangent calculations are demonstrated on the first harmonic peak.)
- Fig. 4. Resonant MD longitudinal moisture-temperature-specific modulus data for 550-P00 cellophane.
- Fig. 5. The 55°C moisture-specific modulus master curve for MD longitudinal measurements on 550-P00 cellophane.
- Fig. 6. Resonant MD longitudinal moisture-temperature-specific modulus data for PUD0-134 cellophane over an extended temperature range.
- Fig. 7. Resonant MD longitudinal moisture-temperature-loss tangent data for PUD0-134 cellophane over the extended temperature range.
- Fig. 8. A reproduction of the low frequency MD longitudinal moisture-temperature-loss tangent data from Bradley and Carr [6] for PUD0-193.
- Fig. 9. A loss tangent and modulus-log frequency plot of a standard linear solid model undergoing a single thermal transition.

TABLE 1  
MOISTURE-TEMPERATURE-MODULUS REGRESSION ANALYSIS

Sample <sup>a</sup> - Technique <sup>b</sup>	Mode <sup>c</sup>	S <sub>y</sub> <sup>d</sup> (km/sec) <sup>2</sup>	r <sup>2</sup>	V <sub>o</sub> <sup>2</sup> (km/sec) <sup>2</sup>	β <sub>M</sub> /V <sub>o</sub> <sup>2</sup> (1/%)	β <sub>T</sub> /V <sub>o</sub> <sup>2</sup> (1/°C)	β <sub>M</sub> /β <sub>T</sub> (°C/%)	M <sub>o</sub> (%)
I-B	SHEAR	0.21	0.979	4.22	-0.067	-0.0065	10.3	10.2
I-A	MDL	0.18	0.995	8.52	-0.057	-0.0050	11.3	10.2
II-A	MDL	0.12	0.995	8.57	-0.072	-0.0061	11.8	10.2
III-B	SHEAR	0.08	0.984	3.43	-0.061	-0.0053	11.4	6.4
III-A	MDL	0.11	0.996	11.38	-0.051	-0.0042	12.2	6.4
IV-C	MDL	0.06	0.987	4.77	-0.056	-0.0039	14.3	6.2
IV-A	MDL	0.04	0.992	4.47	-0.053	-0.0044	12.1	6.2
IV-C	MDL	0.06	0.990	4.65	-0.057	-0.0038	14.8	6.2
IV-A	MDL	0.05	0.987	4.25	-0.053	-0.0041	12.9	6.2
V-B	SHEAR	0.03	0.996	2.67	-0.056	-0.0045	12.6	7.7
V-A	MDL	0.11	0.993	9.66	-0.047	-0.0038	12.2	7.7
V-A	MDL	0.03	0.994	10.39	-0.041	-0.0033	12.4	7.7
V-A	GDL	0.03	0.995	3.89	-0.059	-0.0049	12.0	7.7

<sup>a</sup>I: 550 P00 (unplasticized cellophane); b.w. 55 g/m<sup>2</sup>; thickness 38 μm; BCL.  
<sup>a</sup>II: PUDO-134 (unplasticized cellophane); b.w. 55 g/m<sup>2</sup>; thickness 38 μm; Du Pont.  
<sup>a</sup>III: Commercial typing paper; basis weight 75 g/m<sup>2</sup>; thickness 100 μm.  
<sup>a</sup>IV: Commercial blotter stock; basis weight 256 g/m<sup>2</sup>; thickness 600 μm.  
<sup>a</sup>V: Commercial linerboard; basis weight 26#/1000 ft<sup>2</sup> (127 g/m<sup>2</sup>); thickness 240 μm.  
<sup>b</sup>A: Strip resonance.  
<sup>b</sup>B: Sheet time of flight.  
<sup>b</sup>C: Strip time of flight.  
<sup>c</sup>MDL: Machine direction longitudinal.  
<sup>c</sup>CDL: Cross machine direction longitudinal.  
<sup>d</sup>Standard error in the Y estimate.

TABLE 2  
MEASURED MOISTURE RANGES

Sample <sup>a</sup>	$\Delta M$ @ 25°C (%)	$\Delta M$ @ 55°C (%)	$\Delta M$ @ 85°C (%)
I	8-22	3-16	2-9
II	8-14	2-12	1-8
III	5-14	2-9	1-6
IV	6-12	3-11	1-6
V	6-16	4-11	2-8

<sup>a</sup>Same designation as Table 1.

TABLE 3

ROOM TEMPERATURE MOISTURE-MODULUS REGRESSION ANALYSIS FOR PUBLISHED DATA

Sample <sup>a</sup>	Mode <sup>b</sup>	Frequency <sup>c</sup> (kHz)	r <sup>2d</sup>	E <sub>o</sub> <sup>2</sup> (d/cm <sup>2</sup> )	β <sub>M</sub> /E <sub>o</sub> <sup>2</sup> (1/%)	Delta M (%) <sup>M</sup>	M <sub>o</sub> <sup>d</sup> (%)
VI	MDL	Low	{0.990}	4.15	-0.071	2-18	{7.70}
VII	MDL	Low	{0.999}	6.07	-0.065	4-14	{7.70}
VII	CDL	Low	{0.994}	2.89	-0.071	4-14	{7.70}
VIII	MDL	Low	{0.998}	5.28	-0.065	4-14	{7.70}
VIII	CDL	Low	{0.995}	2.10	-0.076	4-14	{7.70}
IX	HSL	0.2	0.992	2.45	-0.073	0-12	6.95
X	HSL	Low	0.981	6.35	-0.053	4-17	6.89
XI	MDL	Low	{0.941}	4.40	-0.050	0-20	{7.70}
XII	MDL	Low	0.997	4.71	-0.063	3-14	6.24
XII	MDL	57	0.994	6.27	-0.045	3-14	6.24
				V <sub>o</sub> <sup>2</sup> (km/sec) <sup>2</sup>	β <sub>M</sub> /V <sub>o</sub> <sup>2</sup> (1/%)		
XII	MDL	57	0.990	9.83	-0.043	3-14	6.24
XII	CDL	57	0.994	6.92	-0.047	3-14	6.24
XII	SHEAR	57	0.996	2.90	-0.048	3-14	6.24
XIII	MDL	5	{0.995}	11.09	-0.041	0-20	{7.70}
XIII	CDL	5	{0.993}	4.19	-0.044	0-20	{7.70}
XIV	HSL	10	{0.918}	6.19	-0.011	4-18	{6.95}
XV	MDL	60	0.994	10.99	-0.041	5-12	7.75
XV	CDL	60	0.991	4.24	-0.052	5-12	7.75
XV	SHEAR	60	0.985	2.63	-0.044	5-12	7.75

<sup>a</sup>VI: Kraft eucalypt [19].  
<sup>a</sup>VII: Lake States linerboard [26].  
<sup>a</sup>VIII: Southern linerboard [26].  
<sup>a</sup>IX: Bleached sulfite (215 g/m<sup>2</sup>; 256 μm) [25].  
<sup>a</sup>X: Softwood alpha (56 g/m<sup>2</sup>; 75 μm) [27].  
<sup>a</sup>XI: Kraft sack (105 g/m<sup>2</sup>; 182 μm) [20].  
<sup>a</sup>XII: Bond (75 g/m<sup>2</sup>; 112 μm) [28].  
<sup>a</sup>XIII: Kraft linerboard (186 g/m<sup>2</sup>) [23].  
<sup>a</sup>XIV: Bleached sulfite (60 g/m<sup>2</sup>) [29].  
<sup>a</sup>XV: Linerboard (337 g/m<sup>2</sup>; 527 μm) [30].  
<sup>b</sup>MDL: Machine direction longitudinal.  
<sup>b</sup>CDL: Cross machine direction longitudinal.  
<sup>b</sup>HSL: Handsheet longitudinal.  
<sup>c</sup>LOW: (Initial slope of stress-strain curves).  
<sup>d</sup>{ }: Estimated.

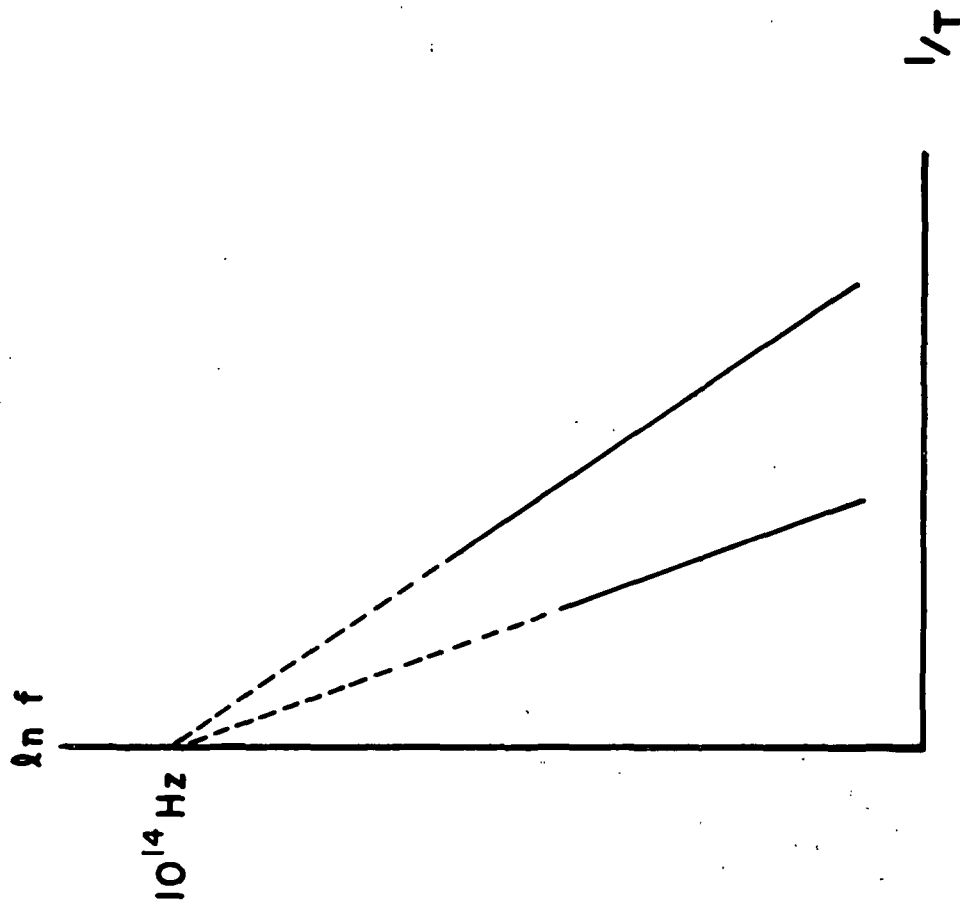


Fig. 1. A hypothetical Arrhenius plot for a viscoelastic material with two thermal relaxations.

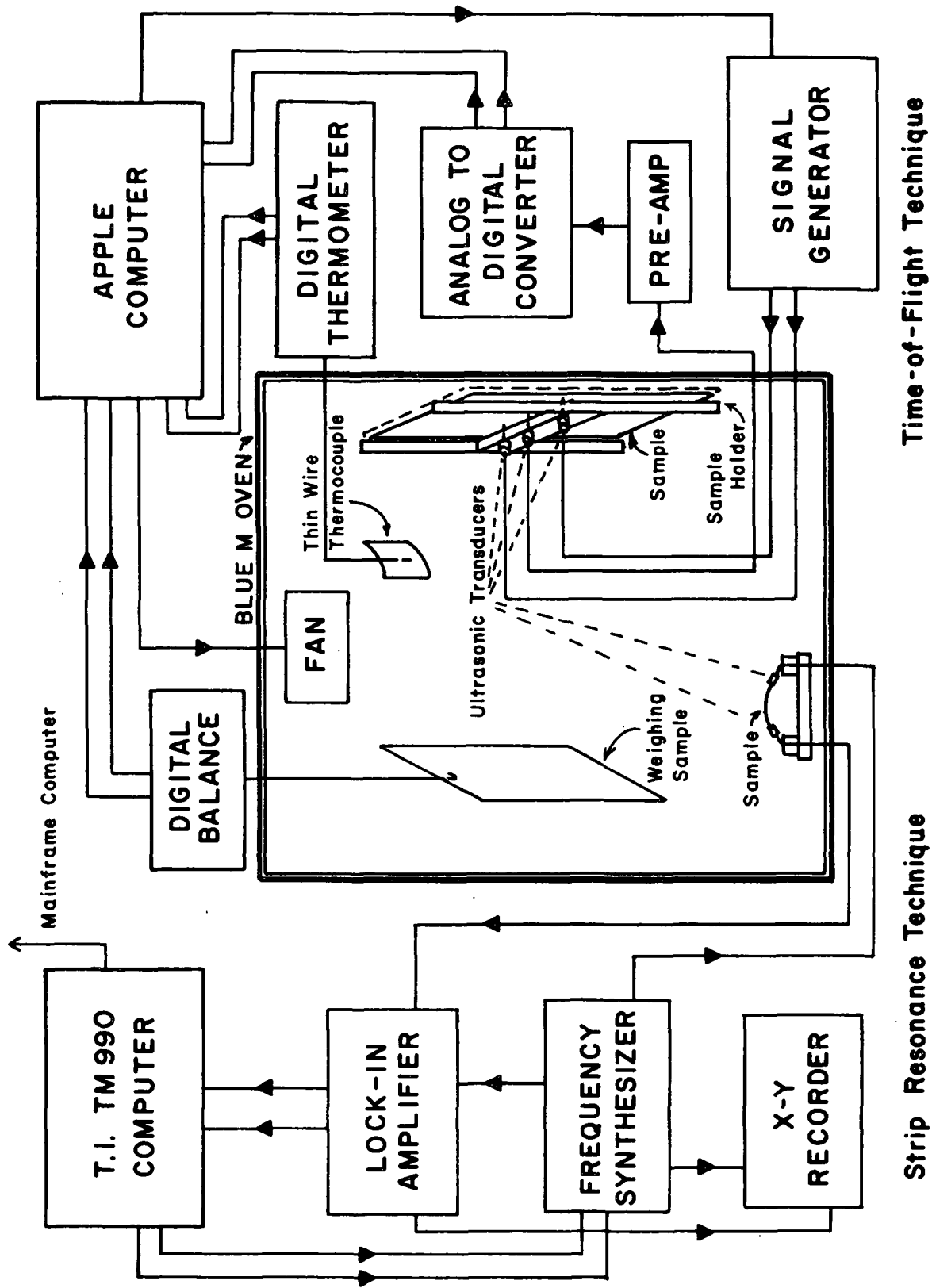


Fig. 2. A schematic of the resonant and time-of-flight experiments enclosed in the variable humidity oven.

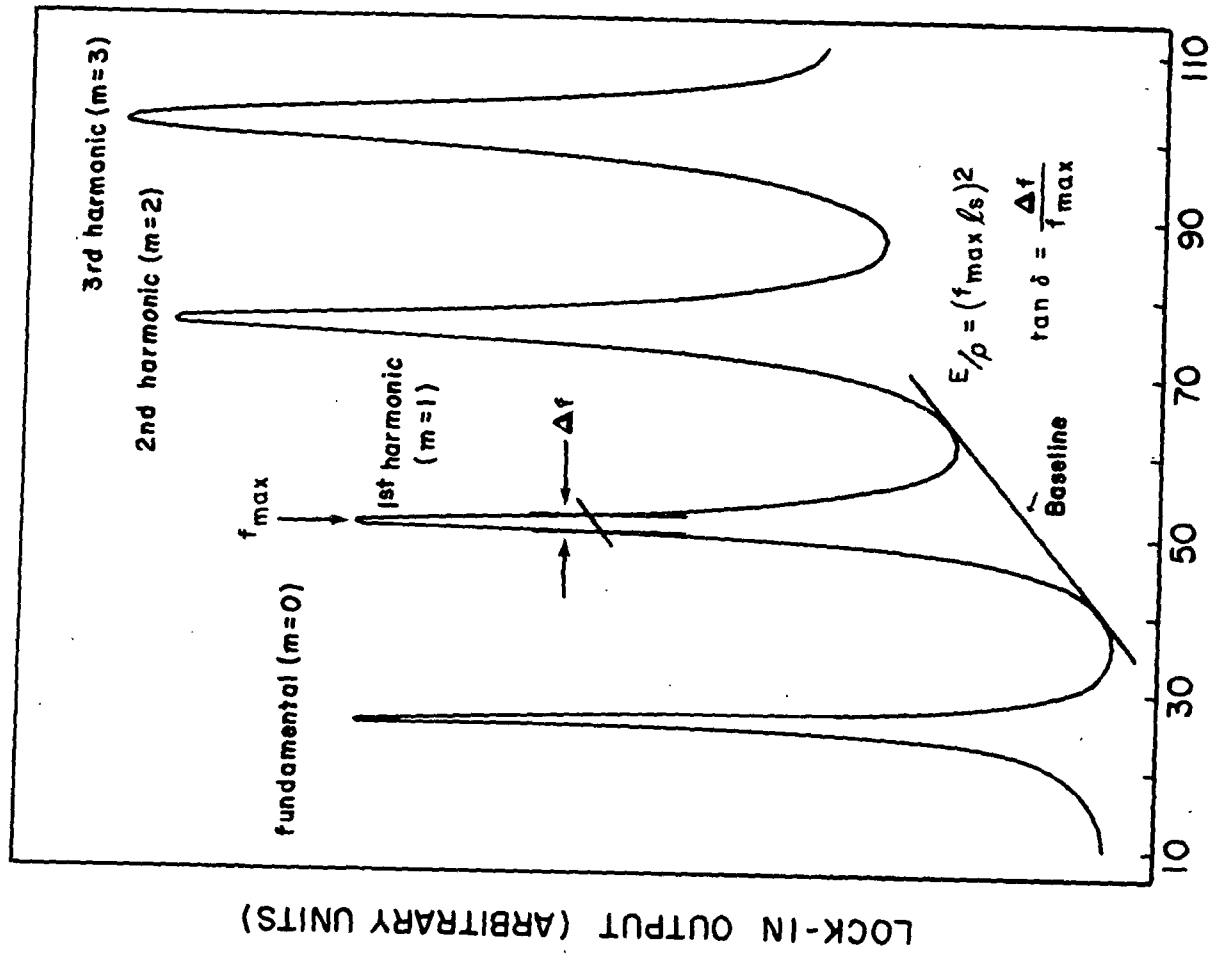


Fig. 3. A typical trace from the X-Y plotter of the lock in amplifier response as a function of frequency. (The methods used for the modulus and loss tangent calculations are demonstrated on the first harmonic peak.)

# UNPLASTICIZED CELLOPHANE(550 P00)

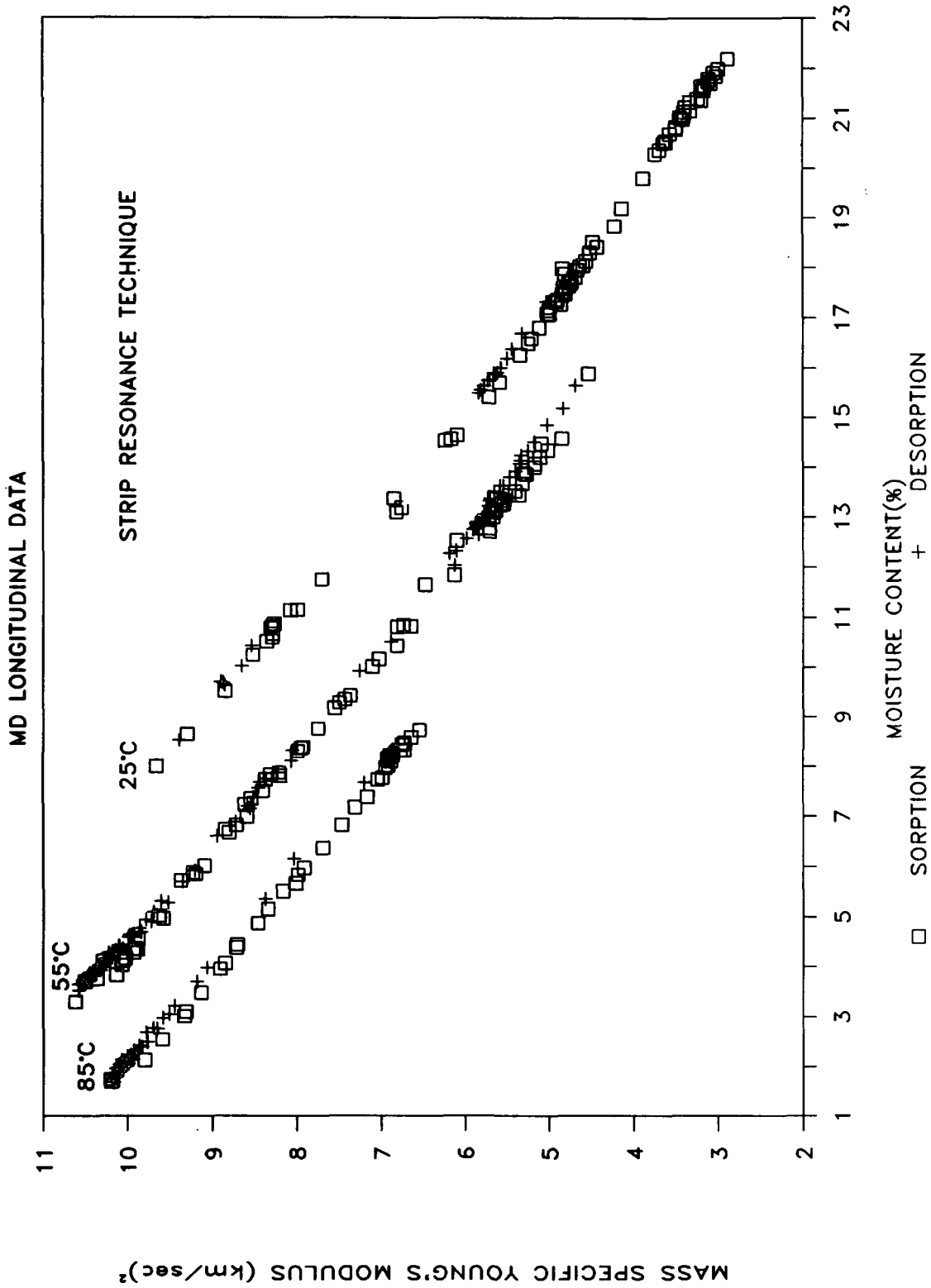


Fig. 4. Resonant MD longitudinal moisture-temperature-specific modulus data for 550-P00 cellophane.

# UNPLASTICIZED CELLOPHANE(550 P00)

MD LONGITUDINAL NORMALIZED TO 55°C

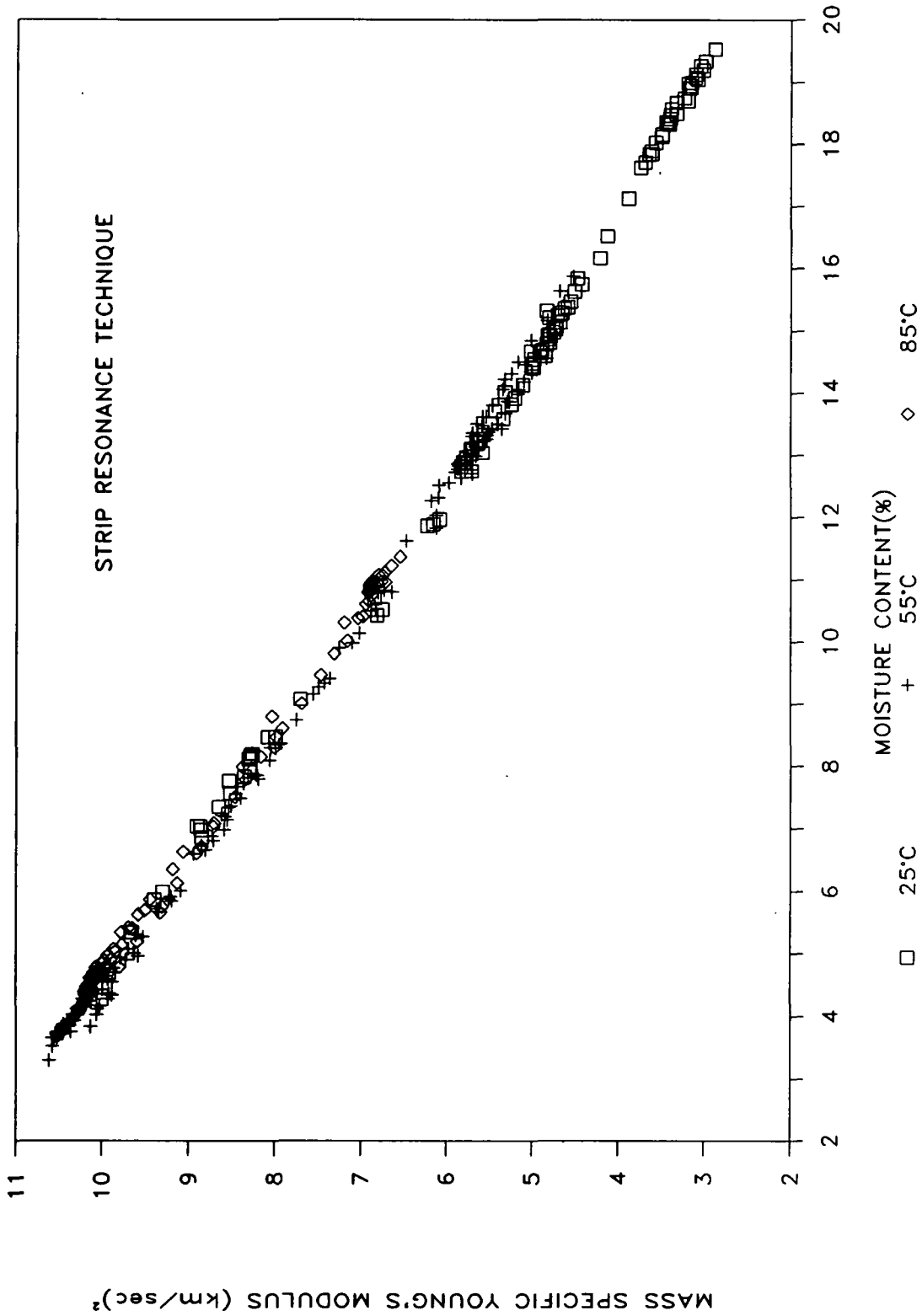


Fig. 5. The 55°C moisture-specific modulus master curve for MD longitudinal measurements on 550-P00 cellophane.

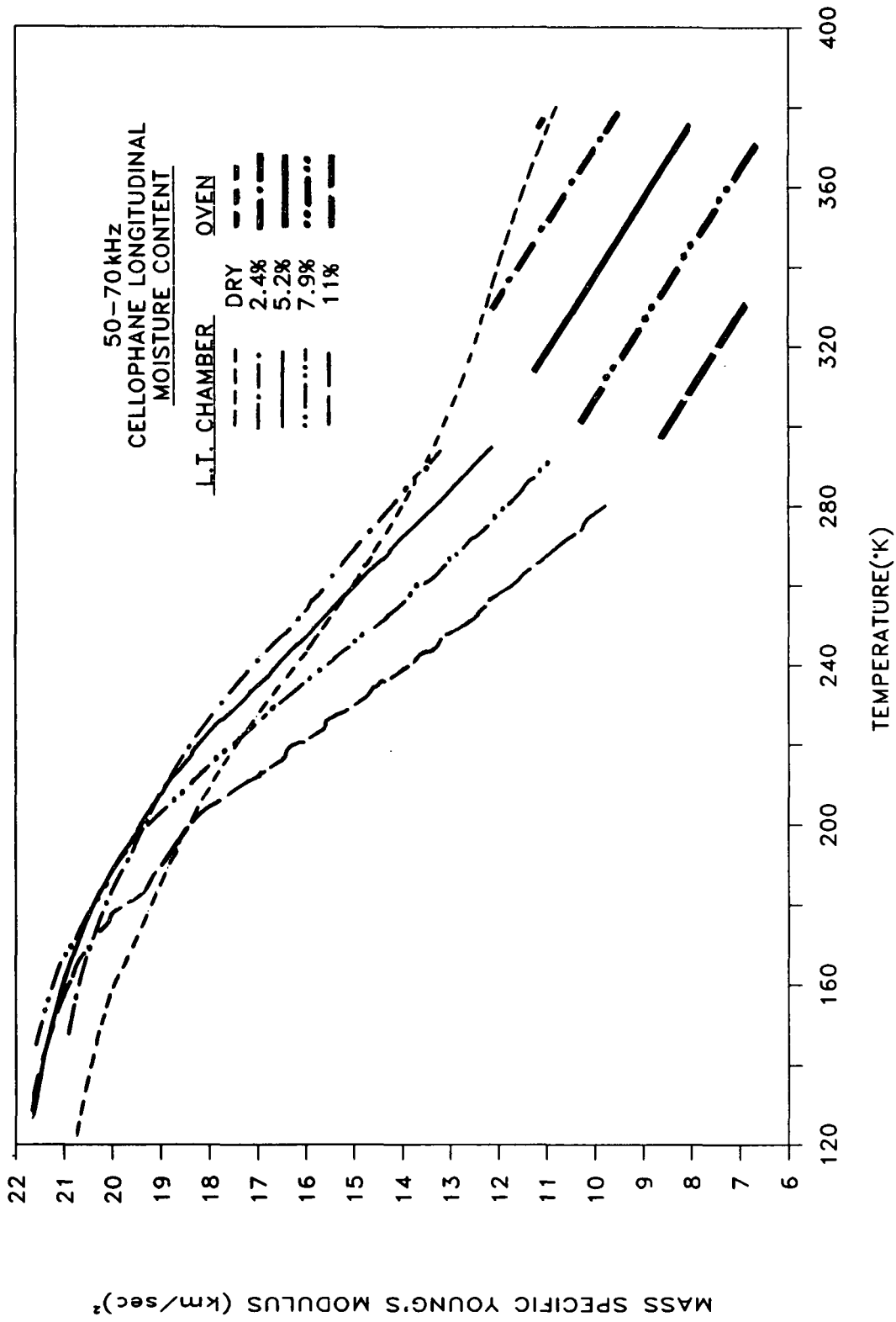


Fig. 6. Resonant MD longitudinal moisture-temperature-specific modulus data for PUD0-134 cellophane over an extended temperature range.

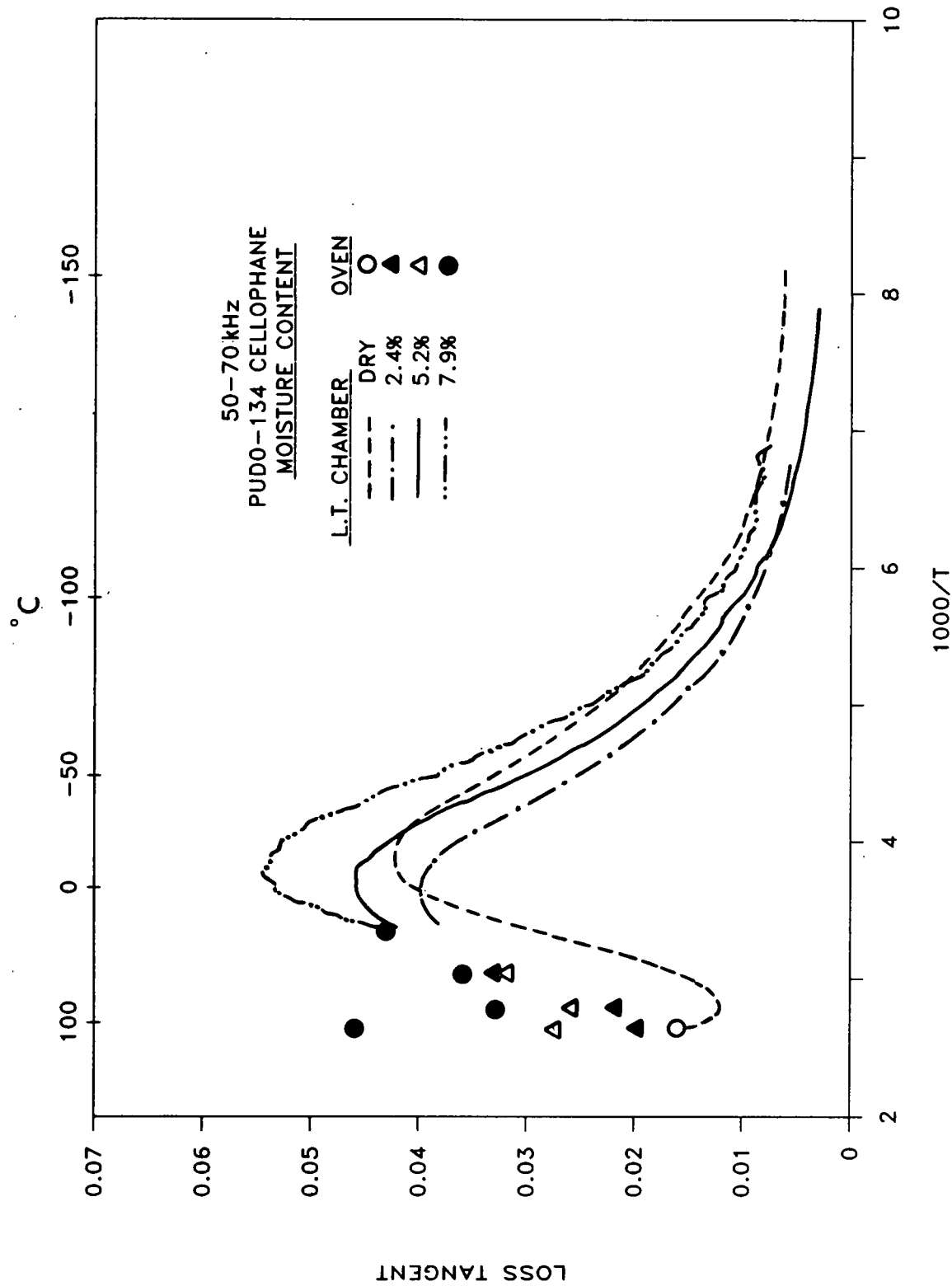


Fig. 7. Resonant MD longitudinal moisture-temperature-loss tangent data for PUD0-134 cellophane over the extended temperature range.

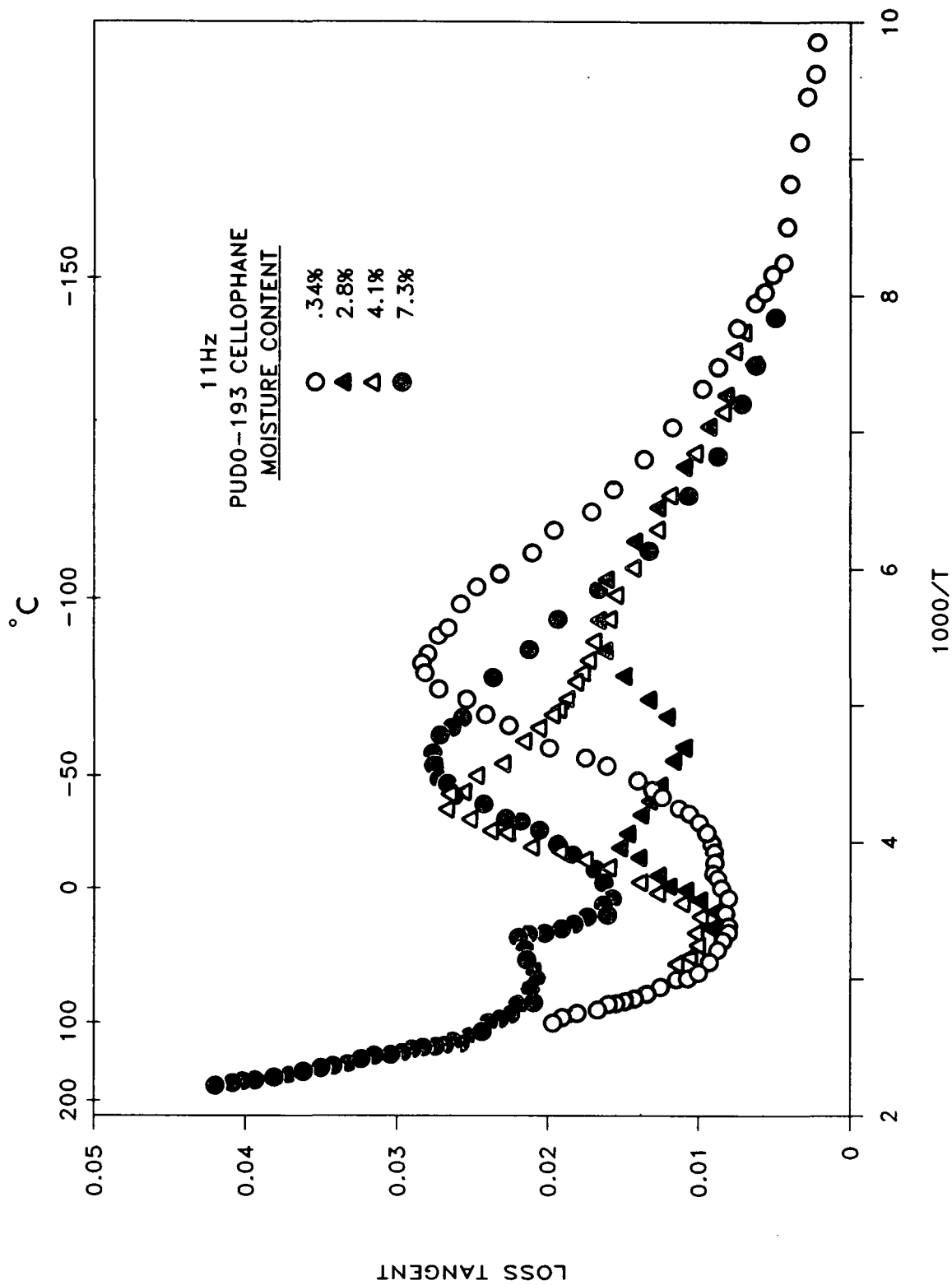
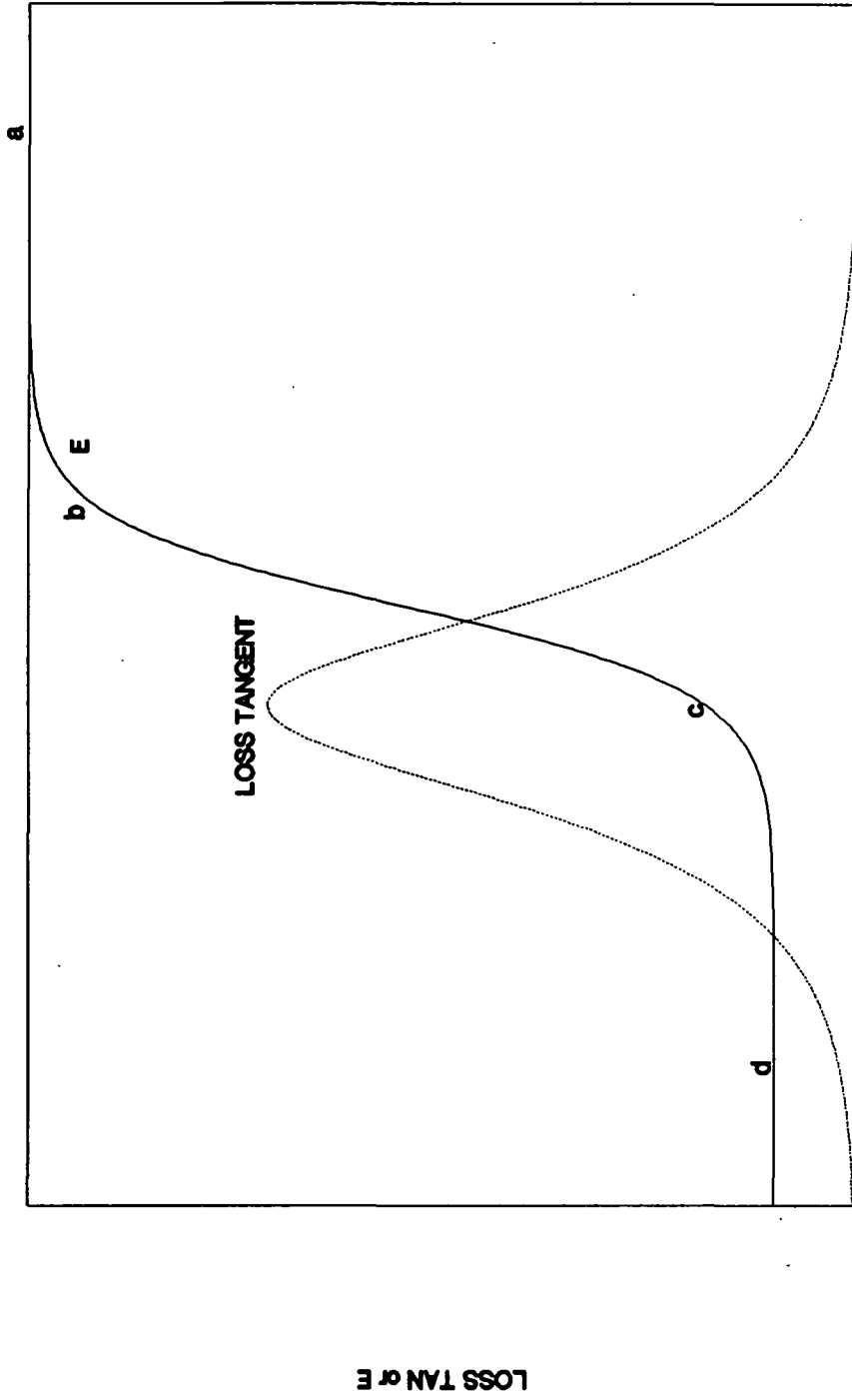


Fig. 8. A reproduction of the low frequency MD longitudinal moisture-temperature-loss tangent data from Bradley and Carr [6] for PUDO-193.

# STANDARD LINEAR SOLID MODEL



LOG FREQUENCY

Fig. 9. A loss tangent and modulus-log frequency plot of a standard linear solid model undergoing a single thermal transition.